





Design and Experimental Characterization of a Shoulder-Elbow Exoskeleton With Compliant Joints for Post-Stroke Rehabilitation

Emilio Trigili , Simona Crea , Matteo Moisè, Andrea Baldoni , Marco Cempini ,
 Giorgia Ercolini, *Member, IEEE*, Dario Marconi, Federico Posteraro,
 Maria Chiara Carrozza, *Member, IEEE*, and Nicola Vitiello, *Member, IEEE*

Abstract—This paper presents the design and experimental characterization of a 4-degree-of-freedom shoulder-elbow exoskeleton, NeuroExos Shoulder-elbow Module (NESM), for upper-limb neurorehabilitation and treatment of spasticity. The NESM employs a self-aligning mechanism based on passive rotational joints to smoothly self-align the robot's rotational axes to the user's ones. Compliant yet high-torque series-elastic actuators allow the NESM to safely interact with the user, particularly in response to sudden unpredicted movements, such as those caused by spastic contractions. The NESM control system provides a variety of rehabilitation exercises, enabling the customization of therapy to patients exhibiting a range of movement capabilities. Available exercises include passive mobilization, active-assisted, active-resisted, and active-disturbed training modes. The experimental characterization of two NESM actuation units demonstrated position and torque control performance suitable for use in neurorehabilitation

Manuscript received July 30, 2018; revised January 18, 2019; accepted March 16, 2019. Date of publication May 24, 2019; date of current version August 14, 2019. Recommended by Technical Editor Prof. Pinhas Ben-Tzvi. This work was supported in part by Regione Toscana within the EARLYREHAB Project (Health Regional Research Programme 2009) and within the RONDA Project (Par Fas 2007-2013 Bando Fas Salute 2014 Regione Toscana. Cup J22116000180002), and in part by the European Union within the Adaptive Integrated Driver-vehicle InterfacE (AIDE) Project (H2020-ICT-22-2014) under Grant 645322 and within the HUMAN MANufacturing (HUMAN) Project (H2020-FOF-2016) under Grant 723737. (E. Trigili and S. Crea equally contributed to this work.) (Corresponding author: Emilio Trigili.)

E. Trigili, A. Baldoni, and D. Marconi are with the BioRobotics Institute, Scuola Superiore Sant'Anna, 56025 Pontedera, Italy (e-mail: emilio.trigili@santannapisa.it; andrea.baldoni@santannapisa.it; dario.marconi@santannapisa.it).

S. Crea, M. C. Carrozza, and N. Vitiello are with the BioRobotics Institute, Scuola Superiore Sant'Anna, 56025 Pontedera, Italy and also with the IRCCS Fondazione Don Carlo Gnocchi, 20148 Milan, Italy (e-mail: simona.crea@santannapisa.it; chiara.carrozza@santannapisa.it; nicola.vitiello@santannapisa.it).

M. Moisè, M. Cempini, and G. Ercolini were with the BioRobotics Institute, Scuola Superiore Sant'Anna, 56025 Pontedera, Italy (e-mail: matteo.moise@iuvo.company; mcempini@gmail.com; giorgiaercolini7@gmail.com).

F. Posteraro is with the Rehabilitation Bioengineering Laboratory, 56048 Volterra, Italy, and also with the Rehabilitation Department, Versilia Hospital, USL Nord Ovest Toscana, 55049 Viareggio, Italy (e-mail: federico.posteraro@uslnordovest.toscana.it).

This paper has supplementary downloadable material available at <http://ieeexplore.ieee.org>, provided by the author.

Color versions of one or more of the figures in this paper are available online at <http://ieeexplore.ieee.org>.

Digital Object Identifier 10.1109/TMECH.2019.2907465

applications, including up to 7 Hz of bandwidth in torque control. An algorithm for online detection of spastic contractions or sudden object collisions has been implemented and tested as well, with results suggesting that the current system can ensure safe interaction with patients.

Index Terms—Robotic rehabilitation, series elastic actuator, spasticity, upper-limb exoskeleton.

I. INTRODUCTION

CARDIOVASCULAR and neurological diseases such as stroke and multiple sclerosis are the main causes of permanent neurological damage [1], [2], and every year millions of stroke survivors need strenuous rehabilitation interventions to recover any degree of motor function. In recent years, robotic devices have gained momentum in the rehabilitation field, due to their benefits of easing the physical burden on physicians and enhancing the precision and intensity of rehabilitation treatments [3], [4].

Robotic devices for rehabilitation can be grouped into three main architectures, according to their physical human-robot interfaces (pHRI): 1) end-point manipulators, which interact with the user at the end-effector level—i.e., the hand and wrist [5], [6]; 2) cable suspensions, in which the affected limb is mobilized with cables driven by motors fixed to a stationary frame [7]–[9]; 3) powered exoskeletons, comprising kinematic chains acting in parallel to the affected limb segments, with a direct correspondence between human articulations and robotic joints. Despite their higher mechanical complexity relative to other architectures, exoskeletons have the ability to act independently on each joint, thus reproducing precise functional movements that can promote cortical reorganization and motor recovery without jeopardizing the natural coordination patterns [10], [11]. Numerous upper-limb exoskeletons have been developed in the past years [12], [13], some of which have become commercially available devices, regularly adopted by clinical rehabilitation centers. Despite their increasing clinical adoption, open research questions related to the design and control of upper limb exoskeletons persist, warranting further research and development to improve their performance and effectiveness. Among these issues, two main design aspects should be carefully considered to realize effective wearable exoskeletons:

the self-alignment of human and robotic joint axes, and the human-robot interface.

Self-alignment mechanisms: Rigid exoskeletons cannot inherently compensate for the laxity of human joints, and proper mechanisms for joint alignment must be integrated into the kinematic structure. As an example, during arm elevation, the glenohumeral joint (GH) is subjected to translational motions, due to the combination of acromioclavicular (AC) and sternoclavicular joint articulations [14]. Similarly to the shoulder, the elbow's rotational axis undergoes small deviations in the frontal and horizontal planes during flexion–extension movements, whose amplitude depends on human inter- and intra-variability, as well as on activation modality (i.e., passive or active) and wrist orientation (i.e., pronated or supinated) [15]. A safe and comfortable pHRI must guarantee proper alignment between the exoskeletal joint axes and the respective anatomical joint axes in each phase of the movement, in order to avoid generating undesired tangential forces on the soft tissues and articulations. To solve this issue, two main approaches have been pursued. On the one hand, “soft” exoskeletons or “exosuits,” composed of actuators embedded within fabric frames, are easily adaptable to body structures, with very low encumbrance and inertia, high inherent compliance, and intrinsic self-alignment capability. Typically, these systems use electric motors and cable-based transmission, with the cables routed around the user's joints in a tendon-like structure and fixed at different connection points [16], [17]. In some cases, pneumatic muscle actuators (PMAs) have also been used [18]. Despite their high degree of wearability, the narrow bandwidth, and the limited amount of torque that exosuits can deliver make these devices suitable only for the treatment of patients with low or mild spasticity. On the other hand, the more classical robotic approach, exploiting rigid frames for transmission, allows the delivery of higher torques with wider bandwidth. In this case, the joint self-alignment mechanism must integrate passive degrees of freedom (DOFs) to create self-aligning kinematic chains, which automatically compensate for deviations from the correct axes orientation [19]. Despite the increased mechanical complexity, passive DOFs have been used in several upper-limb exoskeletons with different configurations [20]–[22].

Human-robot interface: Compliant human-robot interaction is another key design aspect to consider for treating post-stroke subjects, especially to safely interact with sudden, unpredictable movements of the patient. To achieve this goal, rigid exoskeletons typically integrate compliant actuation units, with fixed or variable impedance. Among these, PMAs have inherent compliance, but they need to be used as antagonist couples to control a single DOF [23], unless the movement is actively controlled in only one direction [24]. Compliant joints can be realized by placing an elastic element (a spring) in series with the motor-reduction stage, thus constituting a series-elastic actuator (SEA) [22], [25]–[27]. The elastic component reduces the actuator's mechanical stiffness and reflected inertia in case of sudden movements, and it can function simultaneously as to measure torque.

This paper presents the NeuroExos Shoulder-elbow Module (NESM), an upper-limb exoskeleton for the rehabilitation of

the shoulder and elbow. The main novelty introduced by this device is a self-aligning kinematic chain featuring passive rotational DOFs embedded in the exoskeleton support structure, which allow smooth alignment of the robot shoulder with the rotation axis of the user's shoulder complex, within a workspace that covers the natural translations of the GH joint. In addition, distinctly from other state-of-the-art devices, the robot attachments have been designed to address scapular motion as well, resulting in a fully wearable device able to comply with the complex motion of the whole shoulder girdle, without any motor or active control strategy. The NESM is equipped with four compliant yet high-torque SEA units addressing the shoulder and the elbow, which ensure a safe interaction with the user and comply with sudden, unpredicted movements. In a previous version of the device addressing only the elbow motion, a similar approach has been proven suitable for the rehabilitation of post-stroke subjects exhibiting elbow spasticity [27]. Nevertheless, spasticity of the shoulder girdle muscles occurs in most cases in the hemiplegic arm, causing shoulder pain due to a non-physiological muscle contraction (hypertonia), and requiring a safe mobilization of the whole arm [28]. To address these issues, in addition to the SEAs for the mobilization of the shoulder, the design of the NESM places the actuation units proximally to the addressed joint, enclosing the user's arm only on the external and lateral sides. This design facilitates the donning procedures in case of abnormal arm postures, reduces the external encumbrance, and improves the torque transmission with respect to a remote actuation.

The rest of the paper is structured as follows: Section II describes the NESM mechanical structure, SEA architecture, and kinematics. In Section III, results of the experimental characterization of the NESM are presented. Finally, in Section IV, results and future developments are discussed.

II. NEUROEXOS SHOULDER-ELBOW MODULE PLATFORM

The NESM is a shoulder-elbow exoskeleton with SEA units [Fig. 1(a)]. The exoskeleton is mounted on a wheeled platform that makes it easily movable within a clinical facility; the wheeled platform carries a dedicated box housing the control electronics and an aluminum column that supports the exoskeleton and its weight-relief system. The exoskeleton is connected to the support column by means of an articulated parallelogram, which has passive DOFs at both the exoskeleton and column connection points to realize the passive self-alignment kinematic chain. The articulated parallelogram also carries the exoskeleton counterweights.

The exoskeleton integrates four active rotational joints, three at the shoulder and one at the elbow [Fig. 1(b)]. The three shoulder joints feature the following movements: abduction/adduction (sA/A), i.e., the rotation of the arm away from or toward the center of the body, in the frontal plane; shoulder flexion/extension (sF/E), i.e., the rotation of the arm in the sagittal plane; and shoulder intra/extra rotation (sI/E), i.e., the rotation of the forearm around the humeral axis. The elbow joint features the flexion/extension (eF/E), i.e., the rotation of the forearm around the elbow joint. Several passive DOFs and

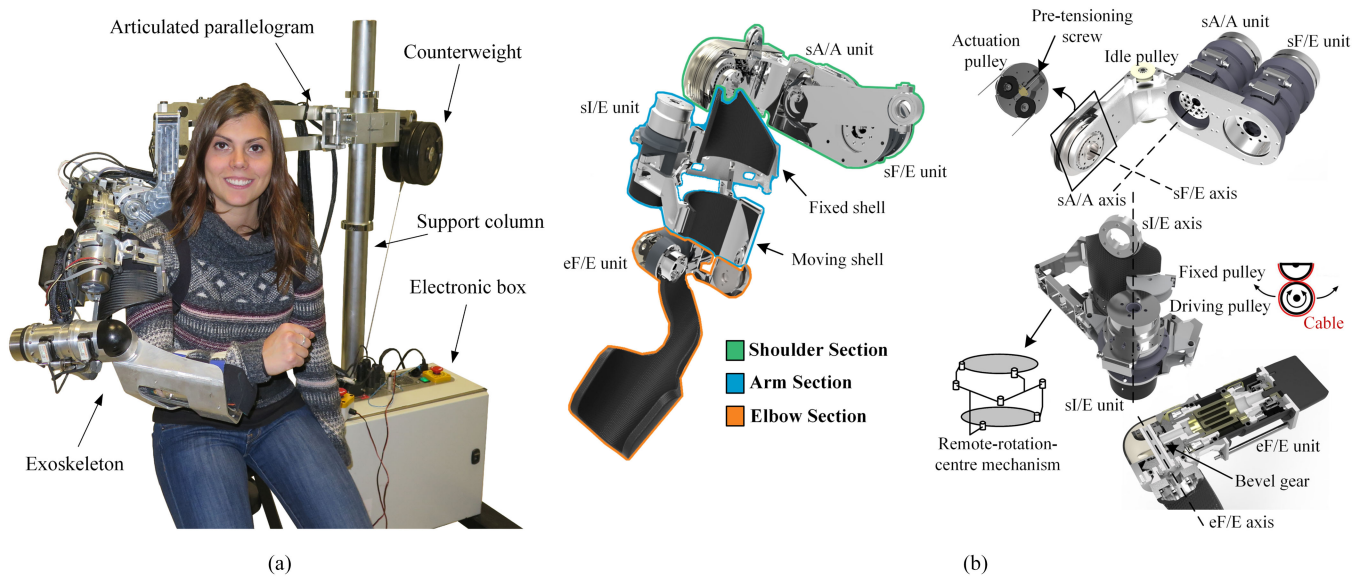


Fig. 1. (a) Overview of the NESM exoskeleton worn by a healthy subject and its support structure. (b) Details of the NESM actuation units.

size adjustment mechanisms have been included for a comfortable and ergonomic fitting of the device [29].

A. Mechanical Structure and Transmission

The NESM device has a modular structure with three main blocks, each one bearing its own actuation units [Fig. 1(b)]. The actuators of the shoulder are configured in series (i.e., sA/A – sF/E – sI/E). This architecture has the advantage of placing the shoulder singularity far from the working space typical of post-stroke rehabilitation exercises. Moreover, the centers of rotation are easy to identify, making the procedure for donning the device quick and easy.

The first block, the *shoulder section* (Fig. 1(b), green contour) comprises drivers and actuators for the sA/A and sF/E joints. An L-shaped aluminum flange spans the user's shoulder and connects the support structure to the exoskeleton. In order to optimize the mass distribution, the two actuation units are placed next to each other, on the rear side of the flange. The sA/A actuation unit has its rotation axis in the anterior–posterior direction, whereas the sF/E rotation is transmitted by means of a cable-pulley stage. Two idle pulleys at the corner of the “L” route the cables from the sF/E actuator to the sF/E actuation pulley, placed on the external lateral side in correspondence of the actual sF/E axis. The pre-tension of the cable can be set by means of a lead-screw mechanism embedded in the actuation pulley. Both sA/A and sF/E actuation units can provide a maximum torque of 60 N·m.

The second block, the *arm section* (Fig. 1(b), blue contour), is dedicated to the sI/E joint. The core structure comprises two coaxial hemi-cylindrical shells rotating around their common axis, intercepting the sF/E and sA/A axes along the humeral direction. The two shells, made in carbon fiber with aluminum inserts, cover the proximal and distal parts of the humerus. The sI/E motion is achieved through an external parallel chain composed of two articulated parallelograms, creating a remote

rotational center of motion. This chain is actuated by means of two capstan pulleys, one driven by the sI/E actuation unit, which is mounted on one linkage of the parallel chain, and the other fixed to the moving shell. A cable is preloaded into a groove and keeps the two pulleys in contact, forcing them to roll on the surface of one another. As a result, the rotation axis is parallel and close to the humeral direction, with its chain running parallel to the user's arm. The main advantage of the proposed solution is that the kinematic chain effecting the sI/E movement covers only the external part of the arm, with a maximum encumbrance diameter equal to only twice the internal hollow diameter, i.e., the internal space for placing the arm. This configuration allows the user to be outfitted with the system from the outside without any difficult maneuvers, so that patients with muscle hypertonia or spastic limbs can easily wear the device. A more detailed description of the kinematics of the sI/E joint can be found in [29].

The third block, the *elbow section* (Fig. 1(b), orange contour), includes the elbow joint. The actuation unit is a cylindrical structure mounted next to the user's elbow and is placed on the external side of the user arm. To reduce the lateral encumbrance, the actuator lies in the sagittal plane, and two bevel gears (ratio 1:1) rotate the final actuation axis by 90° to render it parallel to the anatomical elbow axis.

Table I reports the weight of the three blocks and their sub-assemblies, estimated from the CAD model of the exoskeleton.

B. SEA Architecture

Each actuation unit is composed of a brushless dc motor and reduction gear coupled with a torsional spring, forming a series-elastic actuator architecture. Notably, the sA/A and sF/E actuation units are identical, as well as sI/E and eF/E, respectively. Two custom springs with different mechanical characteristics have been designed to comply with the stiffness of different anatomical joints, for a safe physical human-robot interaction

TABLE I
MASS DISTRIBUTION OF THE NESM, ESTIMATED FROM THE CAD MODEL

Section	Sub-assembly	Weight (kg)
Shoulder	sA/A and sF/E units, L-shaped flange	7.054
Arm	Fixed shell	0.187
	sI/E unit	1.564
	Moving shell	0.368
Elbow	eF/E unit	2.354
	Forearm link	0.490
TOTAL		12.017

TABLE II
SPECIFICATION OF THE NESM ACTIVE JOINTS

	ROM [°]	Max Torque [N·m]	Transmission	Spring stiffness [N·m/rad]
sA/A	-90:0	60	Rigid	165.8
sF/E	-90:0	60	Cables	165.8
sI/E	-80:25	30	Cables	98.8
eF/E	0:125	30	Rigid	98.8

(Table II). The springs for the sA/A and sF/E joints are identical, with a constant stiffness of 165.8 N·m/rad, and are able to transfer a maximum peak torque of 60 N·m. The torque-deflection characterization curve has a linear behavior up to 40 N·m (deflection angle of about 13°) [30]. The sI/E and eF/E joints are equipped with a smaller torsional spring, bearing a maximum torque of 30 N·m (deflection angle of about 17°), with a stiffness of 98.8 N·m/rad within this range.

The sensing system of the SEA comprises two 32-bit absolute optical encoders (Renishaw RESOLUTE), one measuring the true (robotic) joint angle, and the other measuring the angular displacement of the motor and transmission. The difference between these two angles represents the spring deformation, and thus the joint torque (via the spring constant).

C. Passive Degrees of Freedom and Regulations

Passive DOFs: NESM is endowed with eight passive DOFs. A two-axial rotational joint connects the articulated parallelogram to the support column. The first joint [P_1 in Fig. 2(a)] allows for the movement of the exoskeleton along a circular path in the transverse plane. Given the relatively high path radius (600 mm) and small angular stroke under normal movement conditions ($\sim 10^\circ$), the resulting movement of the exoskeleton can be approximated as a horizontal translation, following the shoulder protraction/retraction movement. The second joint (P_2) allows for the movement of the exoskeleton along a circular path in the parallelogram (vertical) plane. Also in this case, given the relatively high path radius (600 mm) and small angular stroke under normal movement conditions ($\sim 10^\circ$), the resulting movement of the exoskeleton can be approximated as a vertical translation. This passive DOF compensates for the

elevation/depression movements of the GH. A third joint (P_3) connects the parallelogram to the exoskeleton shoulder section and allows the rotation of the device around its vertical axis to follow the user's axial trunk rotations.

In Fig. 2(b), the Denavit–Hartenberg model and parameters of the passive kinematic chain including these joints are shown, in the zero-configuration. This configuration maximizes the effects of joint P_1 for the shoulder protraction/retraction and joint P_3 for the trunk rotation. For the modeling of the articulated parallelogram, an additional joint (P_{2bis}) is represented, with the same range of motion (ROM) as P_2 but in the opposite direction, in order to maintain the vertical orientation of P_3 joint. The passive ROM of the GH joint due to these DOFs is represented in Fig. 2(c). In this representation, joint P_1 moves in the range $[-10, +5]^\circ$ and P_2 (P_{2bis}) in the range $[-5, +10]^\circ$, whereas P_3 moves in the range $[-10, +10]^\circ$, with an initial rotation of 10° in the zero-configuration. These values correspond to the ROM allowed by the passive joints when the exoskeleton is worn by the user. With respect to the zero-configuration, the maximum shoulder elevation is about 11 cm, as well as the maximum shoulder protraction. The passive translation in the medio-lateral direction (i.e., along the global x-axis direction) is in the range $[-7, +6]$ cm.

The exoskeleton is connected to the trunk support via a bar linkage endowed with four passive DOFs: a one-axis rotational joint at the sagittal axis (P_4), coaxial to the sA/A joint, and a spherical joint (P_5) on the trunk support, which is fixed to the user by means of Velcro straps and elastic bands. As shown in Fig. 2(d), the combination of P_4 and P_5 allows a movement of the bar linkage along a circular path to follow the rotation of the scapula in the frontal plane (i.e., upward/downward rotation) during shoulder abduction/adduction. Joint P_5 , which has limited ROM when the trunk support is fixed to the user, has the main role of improving wearability by reducing the constraints on the attachment point to the user. In the design of this DOF, the movement of the AC joint is neglected. This assumption can be considered valid within the ROM of the NESM sA/A joint (90°): according to [18] (Nef and Riener, Shoulder Actuation Mechanism for Arm Rehabilitation, 2008), within this range the AC has a maximum rotation of 5° , starting after 80° of shoulder abduction.

A slider (P_6) allows the elbow translation in the forward/backward direction during the flexion/extension movement. The stroke length of the slider is 150 mm. This DOF is a simplified version of the 4-DOF passive mechanism for the elbow joint in [27], where only the main residual movement of the elbow has been addressed, to reduce the encumbrance of the system.

Size regulations: Five size regulations allow the exoskeleton to fit users with different anthropometries [Fig. 2(a)]. A rack and pinion mechanism (R_1), by means of a crank, allows height adjustment of the device. The second adjustment (R_2) allows device inclination in the frontal plane (from 0° to 45°). The arm cuff can be placed in one of three pre-defined positions (R_3) according to the user's humerus length. A rotational joint (R_4) allows for the tilting of elbow axis, while a translational joint (R_5) in the sagittal plane adjusts its position.

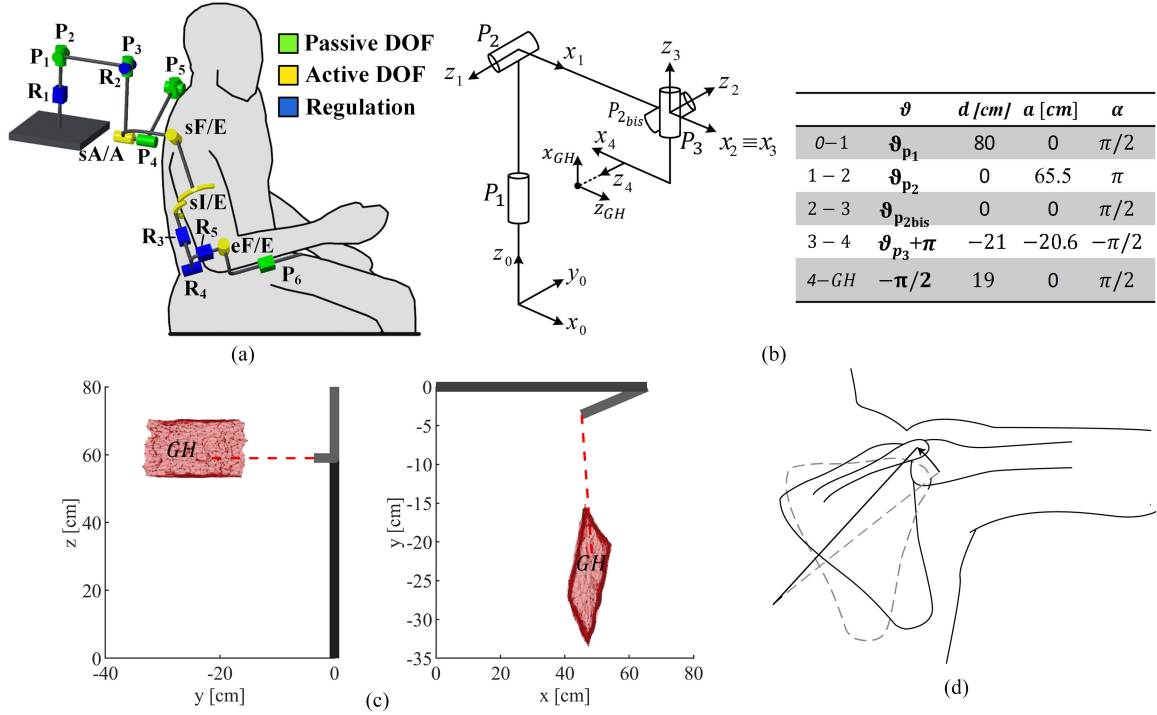


Fig. 2. (a) Kinematic chain of the NESHM including active DOFs, passive DOFs and size regulations. (b) Kinematic model and DH parameter of the passive chain for the shoulder. (c) Three dimensional (3-D) workspace of the shoulder center of rotation (GH) due to the movement of the passive DOFs. (d) Movement of the bar linkage addressing the scapula motion; the initial configuration of the bar and the scapula, with the arm parallel to the user's trunk, is shown in light grey dashed lines.

D. Control System

To enable the adaptation of therapy to users with different residual movement capabilities, the NESHM control system implements two main training paradigms—namely, the robot-in-charge and the patient-in-charge programs [31]. In the robot-in-charge scheme, the robot mobilizes the user's arm along pre-defined reference position trajectories, with joints in *position-control mode*. This program is suitable for patients exhibiting very limited movement capabilities. In the patient-in-charge scheme, the robot's joints operate in *torque-control mode*, enabling the robot either to remain “transparent” to the user's spontaneous movements, or to selectively provide joint torques to assist or resist the user's movement. This program is particularly suitable for the rehabilitation of patients with residual movement capabilities.

To realize the aforementioned paradigms, the control system of the NESHM has been designed with a hierarchical architecture, comprising: 1) a *high-level control layer (HLCL)* delegated to select the desired rehabilitation exercise and generate the corresponding reference position or torque values, and 2) a *low-level control layer (LLCL)* delegated to set and drive the motor currents to follow the desired torque or position values set by the HLCL (Fig. 3).

1) *Low-Level Control Layer*: On the LLCL, the position and torque controller are implemented by means of classical proportional-integrative-derivative (PID) regulators for each of the four active joints. Each controller has been built on the assumption of an independent joint control strategy: the actions on the single joint exerted from the previous ones of the kinematic chain are considered as disturbances to be rejected.

When a joint is position-controlled, the PID regulator operates on the error between the desired joint angle (ϑ_{des}) and measured joint angles (ϑ_j). The output voltage for the motor is controlled via a commercial servo amplifier (Gold Solo Whistle, Elmo Motion Control, Petach Tikva, Israel). In torque-control mode, the input of the PID regulator is the error between the desired torque (τ_{des}) and the measured torque (τ_j). The PID gains were tuned empirically, in order to have a bandwidth around 1 Hz for the position controllers, and to have minimum output impedance in the transparent mode for the torque controllers.

2) *High-Level Control Layer: Patient in charge*: Three different operational modes have been implemented for the patient-in-charge scheme. When the robot is set in *transparent mode*, a reference torque of 0 N·m is commanded to each of the joint controllers, in order to have the minimum output impedance and let the user move freely. By selecting the *impedance control mode*, the system can either: 1) assist the user in following pre-defined joint trajectories, by creating a convergent force field toward the reference trajectory, or 2) apply a divergent force field to disturb the user's movement from following the reference trajectory, according to the following equation:

$$\tau_{des} = k(\vartheta_{ref} - \vartheta_j). \quad (1)$$

In (1), τ_{des} is the setpoint for the low-level torque controller, k is a virtual stiffness (with positive value for a convergent force field and negative for a divergent force field), ϑ_{ref} is the current value of the reference trajectory (i.e., pre-defined angular trajectory the user is requested to follow), and ϑ_j is the measured joint angle.

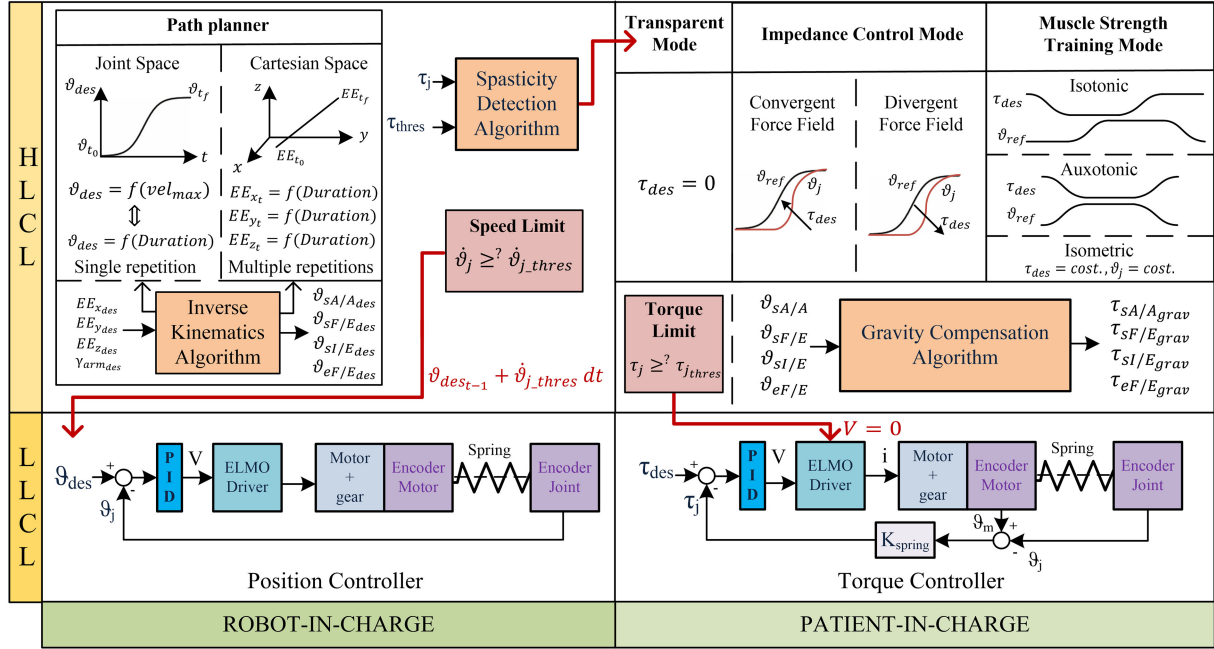


Fig. 3. Hierarchical architecture of the NESM control system. The red arrows indicate the safety measures implemented on the high-level control layer. For the isotonic exercise, a concentric movement training is shown: the resistive torque is kept constant as long as the angle increases, and returns to zero after the concentric movement is completed. Torque and angle variations are always smooth to avoid abrupt changes of forces transmitted to the user.

TABLE III
RISE TIME, SETTLING TIME, AND OVERSHOOT FOR THE TORQUE STEP RESPONSE

	Joint	Rise Time [s]		Settling Time [s]		Overshoot [N·m]	
		Incr. torque	Decr. torque	Incr. torque	Decr. torque	Incr. torque	Decr. torque
Torque Step	sA/A	0.382±0.001	0.377±0.001	0.425±0.001	0.420±0.001	0.036±0.001	0.002±0.002
	eF/E	0.292±0.001	0.303±0.009	0.335±0.001	0.347±0.009	0.006±0.003	0.061±0.026

Finally, in the *muscle strength training mode*, torque is applied on a selected joint to train specific muscular groups. Here, the robot action can realize three different training exercises. In the *isotonic training routine*, a constant resistive torque is commanded to the low-level controller only during the concentric and/or eccentric phases of the target muscle during the movement, as follows:

$$\tau_{des} = \begin{cases} \text{const.} & \text{if } \vartheta_{ref_{min}} < \vartheta_{ref} < \vartheta_{ref_{max}} \\ 0 & \text{otherwise} \end{cases} \quad (2)$$

Both the desired torque for the controller and the reference angle vary following third-order sigmoid functions with null velocity at the beginning ($\vartheta_{ref_{min}}$) and at the end ($\vartheta_{ref_{max}}$) of the movement

$$y(t) = -2 \frac{y_f - y_i}{D^3} t^3 + 3 \frac{y_f - y_i}{D^2} t^2 + y_i \quad (3)$$

In (3), y_f and y_i are the target and initial position (or torque, respectively), and D is the trajectory duration. As an alternative, the trajectory can be expressed as a function of the peak velocity, with the following substitution:

$$D = \frac{3}{2} \frac{y_f - y_i}{V_{peak}} \quad (4)$$

In the *auxotonic training routine*, the desired resistive torque for the low-level controller increases proportionally with the reference angle with respect to a settable zero (τ_0)

$$\tau_{des} = -k\vartheta_{ref} + \tau_0 \quad (5)$$

Finally, in the *isometric training routine*, a constant reference torque is commanded to the low-level controller while the user is asked to maintain a constant position.

In the patient-in-charge scheme, a feed-forward gravity compensation algorithm calculates online the gravity torque of each joint due to the robot weight, according to the dynamic equation

$$\tau = \tau_{des} + g(q) \quad (6)$$

In (4), τ is the vector of joint torques, τ_{des} is the net torque to be applied on the joint, $g(q)$ is the pose-dependent vector of torques due to gravity estimated by the algorithm. The algorithm considers the centers of mass and weights of the mechanical components derived from the CAD model of the exoskeleton, with empirical adjustments [32].

Robot in charge: A path planner based on inverse kinematics (IK) has been developed to set the reference trajectories for the low-level position controllers. The path planner can either calculate the joint's desired positions in joint space or Cartesian

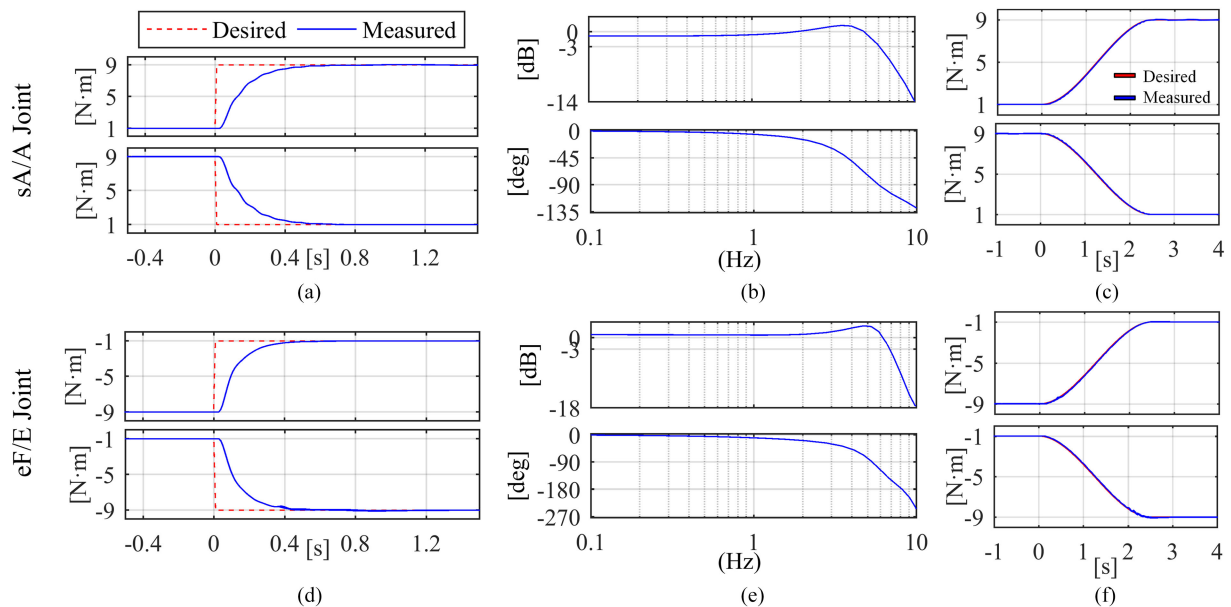


Fig. 4. Closed-loop torque control for the (a)–(c) shoulder adduction/abduction and (d)–(f) flexion/extension joints. (a), (d) Step response for increasing and decreasing steps; the mean value and standard deviation contour calculated over fifty repetitions are represented. (b), (e) Bode diagram (amplitude and phase) of the chirp response mediated over four repetitions. (c), (f). Sigmoid function tracking performance (for increasing and decreasing torques. Each plot reports the mean value and standard deviation contour (lower than 0.02 and 0.08 N·m for sA/A and eF/E, respectively) of the response mediated over fifty repetitions).

space. In the first case, given the desired final end-effector position and arm orientation, an ad-hoc IK algorithm calculates the desired final joint angles (see Appendix in supplementary material available online). In the second case, given the desired final end-effector position and arm orientation, a linear trajectory of the end-effector (roughly corresponding to the hand of the user) is calculated, while the IK algorithm runs at each iteration to drive the joints to the desired end-effector position. In both cases, trajectories are calculated according to (3) and (4), by selecting the maximum joint- or end-effector velocity, or the movement duration from the GUI.

Safety: Different strategies have been implemented on the HLCL to ensure the safety of the user. A rule-based algorithm allows online detection of abnormal torque profiles due to spastic contractions: under the robot-in-charge scheme, if the joint torque velocity overcomes a pre-set threshold, the system automatically switches into transparent mode, to avoid harming the user’s arm. A preliminary version of this spasticity detection algorithm has been presented in [33] for offline applications. In addition, a speed-limit algorithm maintains the maximum speed of the joints below a certain (settable) value. A similar strategy is adopted for the patient-in-charge scheme: in this case, if the measured torque overcomes a pre-set threshold, all the motor drivers are immediately disabled.

III. EXPERIMENTAL CHARACTERIZATION

Different experimental trials have been conducted to characterize the LLCL and HLCL performance.

First, the performances of the LLCL have been assessed for two actuation units, namely the first (sA/A) and last (eF/E) of the kinematic chain (recall, the first- and last two actuators

have identical designs and components). The experimental characterization of the torque and position controllers was conducted in trials that matched the operating conditions of the system in robot-in-charge and patient-in-charge schemes. The performance in tracking position and torque sigmoid trajectories, as well as the step response of the closed-loop torque controller, are reported in the following paragraphs.

In addition, the NESM has been tested in trials with the human in the loop in order to assess its output impedance in the transparent mode and to test the spasticity detection algorithm.

A. Hardware Control Unit

The hardware control unit comprises a real-time controller, sbRIO-9632 (National Instruments—NI, Austin, TX, USA), endowed with a 400-MHz processor running a NI real-time operating system, and a field programmable gate array (FPGA) processor Xilinx Spartan-3. The HLCL runs at 100 Hz on the real-time processing unit, whereas the LLCL runs at 1 kHz on the FPGA level. Notably, for the sF/E joint, an additional absolute rotary magnetic encoder (RLS AksIM) is placed on the actuation pulley (after the cable transmission system) and provides the joint angle value, thus compensating for the intrinsic elasticity of the transmission cable that transfers the output torque from the SEA output to the actual sF/E joint.

B. Characterization of the Torque Controller

Step response: Fifty increasing and decreasing torque steps (amplitude 8 N·m) were commanded, and average values and standard deviations of the rise time, settling time and overshoot were calculated (see Table III). The rise time is lower than 0.4 s for both joints, the settling time is lower than 0.5 and 0.4 s for

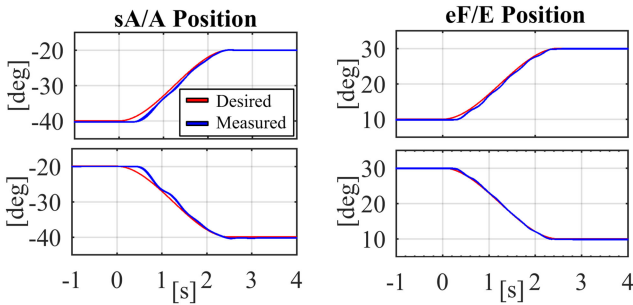


Fig. 5. Tracking performance of the position controller for the sigmoid trajectories of the path planner both for increasing (up) and decreasing (down) angles. Each plot reports the mean value and standard deviation contour (lower than 0.3° and 0.1° for sA/A and eF/E, respectively) of the response mediated over 50 repetitions.

sA/A and eF/E, respectively, whereas the overshoot is lower than 0.04 N·m for sA/A and 0.07 N·m for eF/E. Mean profiles and standard deviation contours (lower than 0.03 and 0.08 N·m for sA/A and eF/E, respectively) of the torque step response are shown in Fig. 4(a), (d).

Chirp response: Four repetitions of a chirp signal with a frequency range between 0.1 and 10 Hz were performed (amplitude 4 N·m, duration 160 s). The amplitude and phase Bode plots of the response mediated over the four repetitions are shown in Fig. 4(b) (sA/A) and Fig. 4(e) (eF/E). The estimated torque bandwidth is 6.1 and 6.9 Hz for sA/A and eF/E, respectively; an overshoot occurs at 4 Hz for sA/A and 5 Hz for eF/E.

Sigmoid torque profiles: Fifty repetitions of a sigmoid torque profile (duration 2.5 s, torque excursion 8 N·m, maximum speed 4.8 N·m/s) were applied to the sA/A and eF/E joints, both for increasing and for decreasing torques [Fig. 4(c), (f)]. For sA/A, the root-mean-squared error (RMSE) between the reference and the measured torque was equal to 0.040 ± 0.001 and 0.038 ± 0.001 N·m, respectively, for increasing and decreasing torque profiles. Similarly, for eF/E the RMSE was equal to 0.046 ± 0.002 and 0.050 ± 0.002 N·m, respectively.

C. Characterization of the Position Controller

For the position controller, the capability to follow the sigmoid trajectories implemented in the path planner has been assessed. Fifty repetitions of a sigmoid angle trajectory (duration 2.5 s, angular excursion 20° , max speed $12^\circ/\text{s}$) were applied to the sA/A and eF/E joints, for increasing and decreasing angles (Fig. 5). For sA/A, the RMSE between reference and measured angle was equal to $0.603^\circ \pm 0.050^\circ$ and $0.609^\circ \pm 0.038^\circ$ for increasing and decreasing angles, respectively. Similarly, for eF/E the RMSE was equal to $0.391^\circ \pm 0.018^\circ$ and $0.186^\circ \pm 0.030^\circ$, respectively.

D. Human-in-the-Loop Tests

Output impedance: One healthy volunteer wore the exoskeleton and performed elbow flexion/extension and shoulder adduction/abduction movements, with the device set in transparent mode and gravity compensation activated. The user was required to move at increasing frequency, following a metronome

(frequency range was set between 0.3 and 2 Hz). The output impedance was calculated as the ratio of the net torque (i.e., the difference between the measured and the gravity torques) and the angle value, normalized for the natural spring stiffness. The results for the sA/A and eF/E joints are shown in Fig. 6. The amplitude of the frequency response at 1 Hz resulted -17 dB for sA/A and -25 dB for eF/E, corresponding to an output impedance value of 23.4 and 5.5 N·m/rad, respectively, meaning that, in transparent mode, sA/A and eF/E joint are, respectively, 7 and 18 times more compliant than the hardware spring stiffness.

Online spasticity detection: A threshold-based algorithm for the detection of abnormal torque profiles due to spastic contractions was implemented and tested. The algorithm is based on two steps: first, a low-pass filter (moving average, with windows of three samples) is applied on the measured joint torque, and then the derivative of the filtered torque is computed. When exceeding a predefined threshold (i.e., 45 N·m/s, as reported in [34]), the corresponding joint automatically switches to transparent mode. The algorithm was tested on four healthy subjects, wearing the exoskeleton controlled in position mode while executing a pre-defined drinking task. A finite-state machine was implemented to perform four sub-tasks: 1) moving to the object; 2) approaching the mouth; 3) bringing the object back to the table; and 4) going to resting position. First, the user performed the whole task five times; then s/he was requested to simulate a sudden unpredicted movement in each one of the sub-tasks, in a random direction. Fig. 7(a) shows the recordings for one of the subjects in a single sub-task (4). In this case, the abrupt change of torque was first detected on the sF/E joint. Fig. 7(b) and (c) shows the deviations from the regular path of the joint angle and joint velocity, as well as the end-effector trajectory. When the change was detected, the difference between the measured torque and the corresponding torque value on the regular task (i.e., without any abnormal movement) was 4.3 , with a delay of 150 ms. The mean torque error and standard deviations for the four subjects at the time of detection were 3.2 ± 1.3 , 5.7 ± 2.4 , 3.6 ± 1.7 , and 3.4 ± 0.6 N·m, respectively.

IV. DISCUSSION

Robotic devices have been recognized as tools to provide high-intensity and repeatable rehabilitation, and improve the engagement of the patient. Two main design requirements have been typically considered for these systems. First, they should include self-alignment mechanisms to ensure that the applied torques are in the correct directions and the system does not cause pain or undesired effects to the user; second they should be able to provide relatively high torques (i.e., up to 20 – 25 N·m) to treat limbs with high spasticity or hypertonia, yet providing a compliant human-robot interface.

A. Kinematics

The kinematic chain of the NESM has been designed to adapt to the residual movement of the shoulder girdle by following shoulder protraction-retraction and elevation-depression translational movements. Residual movements of the elbow, trunk, and scapula can be followed as well. With respect to other

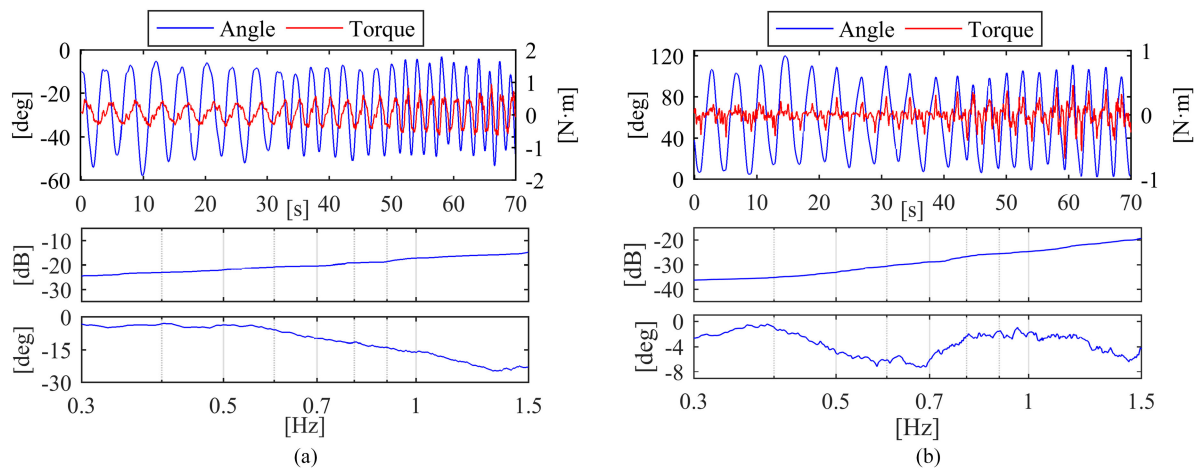


Fig. 6. (a) Output impedance of the shoulder adduction/abduction joint (up); Bode diagrams of the amplitude and phase of the parasitic joint impedance, normalized with respect to the spring natural stiffness of 166 N·m/rad (down). (b) Output impedance of the elbow flexion/extension joint (up); Bode diagrams of the amplitude and phase of the parasitic joint impedance, normalized with respect to the spring natural stiffness of 98 N·m/rad (down).

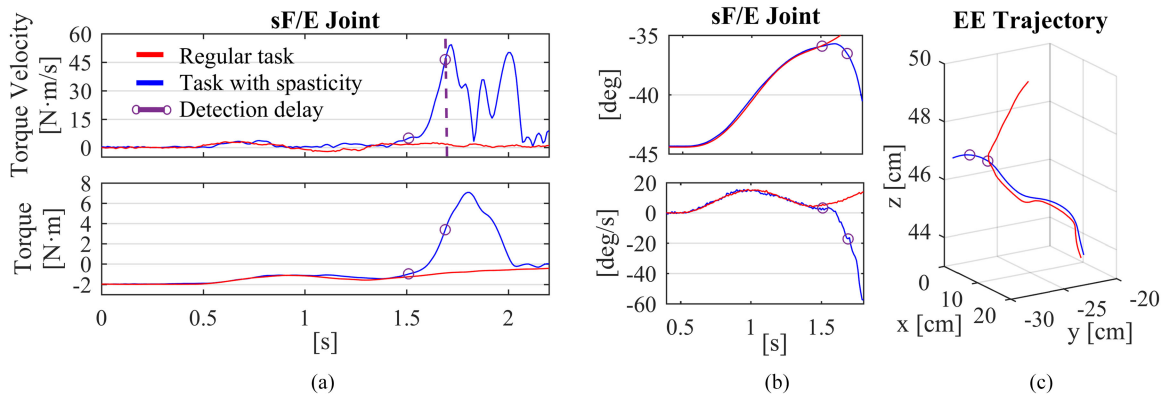


Fig. 7. Comparison between a regular task and the same task with a simulated spastic contraction, executed by passive mobilization of the user's arm. (a) Measured torque profiles (down) and calculated velocity profiles (up). The dotted line corresponds to the actual detection of the spastic contraction (threshold equal to 45 N·m/s). (b) Joint velocity (down) and joint angle (up). (c) End-effector trajectory.

solutions, using active DOFs to counteract the elevation-depression movement [35] or protraction-retraction [20], [36], the NESM addresses both movements by means of passive DOFs, without relying on accurate models to estimate the passive movement. Despite an increase of the overall encumbrance of the system, the passive kinematic chain is embedded within the exoskeleton support structure, and it is able to cover the residual translation of the shoulder center of rotation within the robot shoulder ROM. Indeed, according to [14], the passive shoulder elevation movement is lower than 6 cm for an abduction angle of 90° , whereas the medio-lateral translation has a maximum value of 7 —both compatible with the passive ROM of the NESM shoulder. Similarly, according to [37], the residual anterior translation is lower than 10 cm for a flexion of the shoulder of 90° . For future studies, a complete characterization of the kinematic chain will be carried out with motion tracking systems, to validate the proposed model for complex shoulder motions.

B. Actuation and Safety

The SEA-based architecture of the NESM has been designed to reduce the intrinsic mechanical stiffness of the actuator and

realize an intrinsically safer physical human-robot interface. To meet this requirement, the spring stiffnesses of the NESM joints (165.8 and 98.8 N·m/rad) were chosen to be comparable to the biological joint stiffness [38] and ensure effective shock absorption [39]. To the knowledge of the authors, the only other example of SEA-based shoulder-elbow exoskeleton in the state of the art is the LIMPACT [22]. Similar to the NESM, the LIMPACT actuation units, each including an elastic element with stiffness from 170 to 180 N·m/rad, are able to achieve a maximum torque of 36 N·m. However, the system was specifically designed to provide fast torque perturbations for diagnostics measurements in stroke patients, thus high power hydraulic actuators were used to achieve a torque bandwidth in the range from 43 to 102 Hz. Despite the high performance, the use of hydraulic actuators makes the deployment of the system more difficult in a clinical setting.

Other upper-limb exoskeletons with SEAs have been developed with a smaller number of active DOFs. In [26], a 2-DOF lightweight shoulder exoskeleton with two linear actuators for the shoulder enables the shoulder flexion/extension and adduction/abduction movements. The linear motors are coupled with linear springs of 40 N/mm stiffness. With a maximal force of

220 N for both motors, the maximum pitch torque and yaw torque are 41.69 and 12.99 N·m, respectively. The motorized WREX [40] consists of two passive DOFs for elbow and shoulder rotation in the horizontal plane and two DOFs for elbow and shoulder elevation, actuated in a hybrid setup comprising elastic bands and SEAs (spring stiffness of 2.51 N·m/rad). The torque controller bandwidth is 3.18 Hz. Compared to these devices, the NESM is able to provide higher torques, i.e., up to 30 and 60 N·m for the elbow and shoulder, respectively, with a wider bandwidth, up to 6.9 Hz. These performances are similar to the ARMin III, which can withstand torques up to 38.5 N·m in a bandwidth of 2.2 Hz [14] and the ETS-MARSE, which can deliver up to 54 N·m at the shoulder level [25]—though neither of these devices uses SEAs.

Sensing and reacting to joint forces and torques increases the safety of a wearable device. The online detection of spasms and sudden movements commonly relies on threshold algorithms based on the sensing of the joint torque, as in [27]. Typically, when the measured torque is higher than a set threshold, a spasm is detected and the actuators' desired torque or force is set to zero to release the joints and stop the training [41], [42]. In some cases, more elaborate algorithms employing fuzzy controllers have been developed [43]. By virtue of the high sensing precision provided by the SEA, the NESM control system can implement a simple threshold-based algorithm for online detection of abrupt changes in torque profile (e.g., due to spastic contractions or sudden object collision), and to switch the exoskeleton to transparent mode to avoid harming the user's arm. The threshold on the torque velocity can distinguish the sudden contraction from other circumstances in which the torque increases slowly. The offline analysis of the time delay between the sudden contraction and its detection shows that position measurements can also underline deviations from the regular path before the torque velocity threshold is reached. This supplementary information could be used to include additional thresholds to strengthen the algorithm in real-time applications—for instance, when the rehabilitation exercises are performed in a structured environment with the repetition of functional or stereotyped movements whose trajectories are known *a priori*.

C. Mass Distribution

Except for the slider on the elbow joint, all passive DOFs are located before the exoskeletal arm (i.e., before the chain of active DOFs). This solution has been adopted in order to minimize the weight on the human arm due to the shoulder self-aligning mechanisms. The total weight of the moving arm (around 12 kg) is comparable to other exoskeletons in the state of the art with similar number of active DOFs. The ARMin III shoulder-elbow exoskeleton includes some lockable passive joints in the kinematic chain of the shoulder to provide vertical translation of the GH joint according to the user's anthropometry and has a total weight of 18.755 kg [14]. The LIMPACT has a lower weight (8 kg) thanks to the lightweight hydraulic actuators and hollow aluminum linkages [22]. Despite having a higher

number of active DOFs with respect to the NESM, the ETS-MARSE [25], and the MGA [44] exoskeletons have a total weight of 11 and 10 kg, respectively, but they do not include shoulder self-aligning mechanisms.

The maximum gravity torques, in static conditions, due to the device weight resulted around 14.8, 15.7, 3.1, and 0.9 N·m for sA/A, sF/E, sI/E, and eF/E, respectively [32], meaning that up to 25% of the maximum continuous torque (particularly for sA/A and sF/E) is required to compensate for the weight of the device. Notably, gravity compensation is paramount to reduce the output impedance of the joints at relatively low movement speeds. While the compensation of inertia and Coriolis forces can further improve the system transparency, in our applications we foresee the execution of rehabilitation exercises at relatively low speeds, thus we considered dynamic effects to be negligible [45]. This is in part confirmed by the assessment of the joints output impedance (calculated on the net torque delivered to the joint after gravity compensation), which resulted in being relatively low with movements up to 1.5 Hz. Algorithms for inertia compensation will be implemented for future applications in which higher frequency movement will be executed.

D. Rehabilitation Perspectives

Common robot-based rehabilitation protocols provide passive, active, or “assist-as-needed” arm mobilization exercises. Similar to other devices from the state of the art, such as the variable-stiffness elastic actuated AVSER [46], or the impedance- or force controlled ALEX [47] exoskeletons, the NESM implements different control strategies both for the patient-in-charge and for the robot-in-charge control schemes.

The patient-in-charge modes implemented on the NESM can be personalized according to the user's needs and motion capabilities, to generate assistive or resistive force fields of different intensity and duration, with visual feedback to keep the user engaged the whole time. In the muscle strength training modes, a single joint can be trained in different conditions so that a specific set of muscles (i.e., those involved in the movement of a specific DOF) are strengthened. Finally, the path planner with IK in the robot-in-charge scheme allows replication of task-oriented functional movements for patients with poor residual motion capabilities. Future studies will focus on the clinical validation of the device with post-stroke patients with different levels of spasticity and functional disability.

ACKNOWLEDGMENT

The authors would like to thank Mario Cortese who contributed to the development of the NESM electronic board. Authors S. Crea, M. Moisè, A. Baldoni, M. C. Carrozza, and N. Vitiello have interests in a spin-off company (IUVO S.r.l.) developing and commercializing exoskeleton technology that may benefit in the future from research presented in this paper. The IP protecting the NESM technology has currently been licensed to IUVO S.r.l.

REFERENCES

- [1] G. Thrift *et al.*, "Global stroke statistics," *Int. J. Stroke*, vol. 9, no. 1, pp. 6–18, 2014.
- [2] N. Townsend *et al.*, "Cardiovascular disease in Europe: epidemiological update 2016," *Eur. Heart J.*, vol. 37, no. 42, pp. 3232–3245, 2016.
- [3] G. Turchetti *et al.*, "Why effectiveness of robot-mediated neurorehabilitation does not necessarily influence its adoption," *IEEE Rev. Biomed. Eng.*, vol. 7, pp. 143–153, Jan. 2014.
- [4] J. M. Veerbeek, A. C. Langbroek-Amersfoort, E. E. H. van Wegen, C. G. M. Meskers, and G. Kwakkel, "Effects of robot-assisted therapy for the upper limb after stroke: A systematic review and meta-analysis," *Neurorehabilitation Neural Repair*, vol. 31, no. 2, pp. 107–121, 2017.
- [5] J. Reinkensmeyer *et al.*, "Understanding and treating arm movement impairment after chronic brain injury: Progress with the ARM guide," *J. Rehabil. Res. Develop.*, vol. 37, no. 6, pp. 653–662, 2000.
- [6] H. I. Krebs *et al.*, "Rehabilitation robotics: Pilot trial of a spatial extension for MIT-Manus," *J. NeuroEngineering Rehabil.*, vol. 1, no. 5, 2004.
- [7] H. A. Stienen *et al.*, "Dampac: Dynamic force-coordination trainer for the upper extremities," in *Proc. IEEE 10th Int. Conf. Rehabil. Robot.*, Noordwijk, The Netherlands, 2007, pp. 820–826.
- [8] DIEGO®, Tyromotion. [Online]. Available: <https://tyromotion.com/en/produkte/diego>
- [9] X. Cui, W. Chen, X. Jin, and S. K. Agrawal, "Design of a 7-DOF cable-driven arm exoskeleton (CAREX-7) and a controller for dexterous motion training or assistance," *IEEE/ASME Trans. Mechatronics*, vol. 22, no. 1, pp. 161–172, Feb. 2017.
- [10] R. C. V. Loureiro, W. S. Harwin, K. Nagai, and M. Johnson, "Advances in upper limb stroke rehabilitation: A technology push," *Med. Biol. Eng. Comput.*, no. 49, pp. 1103–1118, 2011.
- [11] J. W. Krakauer, "Motor learning: Its relevance to stroke recovery and neurorehabilitation," *Current Opinion Neurology*, vol. 19, no. 1, pp. 84–90, 2006.
- [12] P. Maciejasz, J. Eschweiler, K. Gerlach-Hahn, A. Jansen-Troy, and S. Leonhardt, "A survey on robotic devices for upper limb rehabilitation," *J. NeuroEngineering Rehabil.*, vol. 11, no. 3, 2014.
- [13] R. A. R. C. Gopura, D. S. V. Bandara, K. Kiguchi, and G. K. I. Mann, "Developments in hardware systems of active upper-limb exoskeleton robots: A review," *Robot. Auton. Syst.*, vol. 75, pp. 203–220, 2016.
- [14] T. Nef, M. Guidali, and R. Riener, "ARMin III—Arm therapy exoskeleton with an ergonomic shoulder actuation," *Appl. Bionics Biomechanics*, vol. 6, no. 2, pp. 127–142, 2009.
- [15] T. R. Duck, C. E. Dunning, G. J. W. King, and J. A. Johnson, "Variability and repeatability of the flexion axis at the ulnohumeral joint," *J. Orthopaedic Res.*, vol. 21, pp. 399–404, 2003.
- [16] M. Xiloyannis, L. Cappello, K. D. Binh, C. W. Antuvan, and L. Masia, "Preliminary design and control of a soft exosuit for assisting elbow movements and hand grasping in activities of daily living," *J. Rehabil. Assistive Technologies Eng.*, vol. 4, pp. 1–15, 2017.
- [17] D. Park and K.-J. Cho, "Development and evaluation of a soft wearable weight support device for reducing muscle fatigue on shoulder," *PLOS ONE*, vol. 12, no. 3, 2017.
- [18] H. Kobayashi, Y. Ishida, and H. Suzuki, "Realization of all motion for the upper limb by a muscle suit," in *Proc. IEEE Int. Workshop Robot Human Interactive Commun.*, Kurashiki, Okayama, Japan, 2004, pp. 631–636.
- [19] E. E. G. H. Stienen, F. C. T. van der Helm, and H. van der Kooij, "Self-aligning exoskeleton axes through decoupling of joint rotations and translations," *IEEE Trans. Robot.*, vol. 25, no. 3, pp. 628–633, Jun. 2009.
- [20] M. Ergin and V. Patoglu, "ASSISTON-SE: A self-aligning shoulder-elbow exoskeleton," in *Proc. IEEE Int. Conf. Robot. Automat.*, Saint Paul, MN, USA, 2012, pp. 2479–2485.
- [21] N. Vitiello *et al.*, "NeuroExos: A powered elbow exoskeleton for physical rehabilitation," *IEEE Trans. Robot.*, vol. 29, no. 1, pp. 220–235, Feb. 2013.
- [22] Otten *et al.*, "LIMPACT: A hydraulically powered self-aligning upper limb exoskeleton," *IEEE/ASME Trans. Mechatronics*, vol. 20, no. 5, pp. 2285–2298, Oct. 2015.
- [23] N. G. Tsagarakis and D. G. Caldwell, "Development and control of a 'soft-actuated' exoskeleton for use in physiotherapy and training," *Auton. Robots*, vol. 15, pp. 21–33, 2003.
- [24] S. Balasubramanian and J. He, "Adaptive control of a wearable exoskeleton for upper-extremity neurorehabilitation," *Appl. Bionics Biomechanics*, vol. 9, pp. 99–115, 2012.
- [25] M. H. Rahman *et al.*, "Development of a whole arm wearable robotic exoskeleton for rehabilitation and to assist upper limb movements," *Robotica*, vol. 33, no. 1, pp. 19–39, 2015.
- [26] L. Chien, D. Chen, and C. Lan, "Design of an adaptive exoskeleton for safe robotic shoulder rehabilitation," in *Proc. IEEE Int. Conf. Adv. Intell. Mechatronics (AIM)*, Banff, AB, Canada, 2016, pp. 282–287.
- [27] N. Vitiello *et al.*, "Functional design of a powered elbow orthosis toward its clinical employment," *IEEE/ASME Trans. Mechatronics*, vol. 21, no. 4, pp. 1880–1891, Aug. 2016.
- [28] M. P. De Carvalho, D. Pinto, M. Gorayeb, and J. Jacinto, "Analysis of a 15-years' experience in including shoulder muscles, when treating upper-limb spasticity post-stroke with botulinum toxin type A," *Topics Stroke Rehabil.*, vol. 25, no. 3, pp. 194–202, 2018.
- [29] M. Cempini, N. Vitiello, F. Giovacchini, M. Moisè, and M. Cortese, "Ergonomic exoskeleton system for the upper limb," Patent WO2016166652A1, Oct. 20, 2016.
- [30] F. Giovacchini, M. Cempini, N. Vitiello, and M. Carrozza, "Torsional transmission element with elastic response," Patent WO2015001469A1, Jan. 8, 2015.
- [31] J. A. Haarman, J. Reenalda, J. H. Buurke, H. van der Kooij, and J. S. Rietman, "The effect of 'device-in-charge' versus 'patient-in-charge' support during robotic gait training on walking ability and balance in chronic stroke survivors: A systematic review," *J. Rehabil. Assistive Technologies Eng.*, vol. 3, pp. 1–16, 2016.
- [32] S. Crea *et al.*, "Validation of a gravity compensation algorithm for a shoulder-elbow exoskeleton for neurological rehabilitation," in *Converging Clinical Eng. Res. Neurorehabilitation II. Biosystems & Biorobotics*, Springer, Cham, vol. 15, pp. 495–499, 2017.
- [33] S. Crea *et al.*, "A novel shoulder-elbow exoskeleton with series elastic actuators," in *Proc. 6th IEEE Int. Conf. Biomed. Robot. Biomechanics (BioRob)*, Singapore, 2016, pp. 1248–1253.
- [34] Y.-N. Wu *et al.*, "Characterization of spasticity in cerebral palsy: Dependence of catch angle on velocity," *Developmental Med. Child Neurology*, vol. 52, pp. 563–569, 2010.
- [35] H.-S. Park, Y. Ren, and L.-Q. Zhang, "IntelliArm: An exoskeleton for diagnosis and treatment of patients with neurological impairments," in *Proc. 2nd IEEE RAS & EMBS Int. Conf. Biomed. Robot. Biomechanics*, Scottsdale, AZ, USA, 2008, pp. 109–114.
- [36] D. Koo, P. H. Chang, M. K. Sohn, and J. H. Shin, "Shoulder mechanism design of an exoskeleton robot for stroke patient rehabilitation," in *Proc. IEEE Int. Conf. Rehabil. Robot.*, Zurich, Switzerland, 2011, pp. 1–6.
- [37] D. T. Harryman *et al.*, "Translation of the humeral head on the glenoid with passive glenohumeral motion," *The J. Bone Joint Surgery*, vol. 72, no. 9, pp. 1334–43, 1990.
- [38] D. Piovesan, A. Pierobon, P. Di Zio, and J. R. Lackner, "Measuring multi-joint stiffness during single movements: Numerical validation of a novel time-frequency approach," *PLOS ONE*, vol. 7, no. 3, 2012, Art. no. e33086.
- [39] G. A. Pratt and M. M. Williamson, "Series elastic actuators," in *Proc. IEEE/RJS Int. Conf. Intell. Robots Syst. Human Robot Interaction Cooperative Robots*, Pittsburgh, PA, USA, 1995, pp. 399–406.
- [40] D. Ragonesi, S. Agrawal, W. Sample, and T. Rahman, "Series elastic actuator control of a powered exoskeleton," in *Proc. 33rd Annu. Int. Conf. IEEE Eng. Med. Biol. Soc. (EMBS)*, Boston, MA, USA, 2011, pp. 3515–3518.
- [41] X. J. Xiong, R. Sun, X. Huang, and Y. Xiong, "Control methods for exoskeleton rehabilitation robot driven with pneumatic muscles," *Ind. Robot: An Int. J.*, vol. 36, no. 3, pp. 210–220, 2009.
- [42] S. Zhang, S. Guo, B. Gao, H. Hirata, and H. Ishihara, "Design of a novel telerehabilitation system with a force-sensing mechanism," *Sensors*, vol. 15, pp. 11511–11527, 2015.
- [43] L. Pan *et al.*, "Safety supervisor strategy for an upper-limb rehabilitation robot based on impedance control," *Int. J. Adv. Robot. Syst.*, vol. 10, pp. 1–12, 2013.
- [44] J. T. Carignan and S. Roderick, "Development of an exoskeleton haptic interface for virtual task training," in *Proc. The IEEE/RJS Int. Conf. Intell. Robots Syst.*, St. Louis, MO, USA, 2009, pp. 3697–3702.
- [45] M. Bergamasco *et al.*, "An arm exoskeleton system for teleoperation and virtual environments applications," in *Proc. IEEE Int. Conf. Robot. Autom.*, San Diego, CA, USA, 1994, pp. 1449–1454.
- [46] R.-J. Wang and H.-P. Huang, "AVSER-Active variable stiffness exoskeleton robot system: Design and application for safe active-passive elbow rehabilitation," in *Proc. The IEEE/ASME Int. Conf. Adv. Intell. Mechatronics*, Kaohsiung, Taiwan, 2012, pp. 220–225.
- [47] E. Pironcini *et al.*, "Evaluation of the effects of the Arm Light Exoskeleton on movement execution and muscle activities: A pilot study on healthy subjects," *J. NeuroEngineering Rehabil.*, vol. 13, no. 9, 2016.



Emilio Trigili received the Ph.D. degree in biorobotics from the Biorobotics Institute, Scuola Superiore Sant'Anna (SSSA), Pontedera, Italy, in 2019.

His research activities focus on the design and development of control strategies and algorithms for upper-limb exoskeletons, in assistance and rehabilitation scenarios.



Giorgia Ercolini (M'19) received the M.Sc. degree in biomedical engineering from the University of Pisa, Pisa, Italy, in 2016.

She worked as Assistant of Research with the Biorobotics Institute (SSSA), Pontedera, Italy, focusing on the development of control strategies for upper-limb rehabilitation provided by exoskeletons.



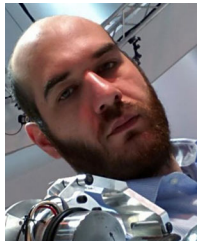
Simona Crea received the Ph.D. degree in biorobotics from The Biorobotics Institute (SSSA), Pontedera, Italy, in December 2015.

She is currently an Assistant Professor with The Biorobotics Institute (SSSA). She is the Project Manager of the H2020 CYBERLEGS Plus Plus project, and co-PI of two national projects funded by INAIL, namely MOTU and Habilis. Her research activities focus on developing and validating novel technologies and paradigms of human-robot interaction for wearable robotics, with particular focus on behavioral aspects.



Dario Marconi received the M.Sc. degree in biomedical engineering from the University of Pisa, Pisa, Italy, in 2015. He is currently working toward the Ph.D. degree at the Biorobotics Institute (SSSA), Pontedera, Italy.

His research activities include the development of control strategies for robot-assisted hand rehabilitation and the assessment of functional requirement for hand exoskeletons



Matteo Moisé received the M.Sc. degree in aerospace engineering from the University of Pisa, Pisa, Italy, in 2011.

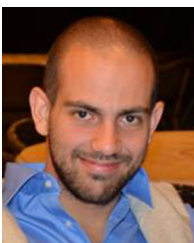
He joined the Wearable Robotics Laboratory, The Biorobotics Institute (SSSA), Pontedera, Italy, as Structural and Mechanical Designer of all wearable robots. He has advanced knowledge of CAD/FEM software and manufacturing technologies. In 2015 he joined the spin-off company IUVO S.r.l. as R&D Engineer.



Federico Posteraro graduated as a Medical Doctor in 1987. He received post-graduated titles as Child Neurologist and Psychiatrist and in Physical Medicine and Rehabilitation, University of Pisa, Pisa, Italy.

He was responsible for Stella Maris Scientific Institute of TREMOR Project in Telematics Application Programme and of H-FORM Project in Horizon Programme. He is currently Head of the Rehabilitation Department, Versilia Hospital, USL north-west, Tuscany, Italy. He is the author or co-author of more than 30 ISI/Scopus papers.

Dr. F. Posteraro has been a member of COST Action European Network on Robotics for NeuroRehabilitation.



Andrea Baldoni received the Ph.D. degree in biorobotics from the Biorobotics Institute (SSSA), Pontedera, Italy, in 2019.

His research interests include the fields of mechanical solutions and innovative technologies.



Maria Chiara Carrozza (M'04) received the M.Sc. degree in physics from University of Pisa, Italy, in 1990, and the Ph.D. degree in engineering from Scuola Superiore Sant'Anna, Pisa, in 1994.

She was a Rector with Biomedical Engineering and Robotics, Scuola Superiore Sant'Anna from 2007 to 2013. In 2013 through 2014 she was the Italian Minister for University, Education and Research. She is currently a Full Professor with Biomedical Engineering and Robotics,

Scuola Superiore Sant'Anna, and Scientific Director of Fondazione Don Carlo Gnocchi, a network of Research Hospitals dedicated to Rehabilitation Medicine. Her research interests are in wearable robotics and rehabilitation engineering.



Marco Cempini received the Ph.D. degree in biorobotics from The Biorobotics Institute (SSSA), Pontedera, Italy, where he also worked as a Postdoctoral fellow.

He has participated in several EU FP7 research projects related to the development of rehabilitation and assistive robotic devices (CYBERLEGS, WAY, EVRYON), with major roles in the mechatronic development. His research interests include mechanical design, modeling, and development of wearable robots.



Nicola Vitiello (M'12) received the Ph.D. degree in biorobotics from The Biorobotics Institute (SSSA), Pontedera, Italy, in 2010.

He is currently an Associate Professor with The Biorobotics Institute (SSSA). Currently he is the Scientific Project Coordinator of the H2020-ICT-CYBERLEGS Plus Plus project, the national project MOTU funded by INAIL, and partner of the H2020-FoF-HUMAN project. He is the author or co-author of more than 60 ISI/Scopus papers, more than 30 peer-review conference proceedings papers, and more than 20 patent applications. His interests include the development, experimental validation and maturation of novel wearable robotic devices for human movement assistance, rehabilitation and augmentation. He is a co-founder of the spin-off company IUVO S.r.l.